

Spin current propagation through ultra-thin insulating layers in multilayered ferromagnetic systems

C. Swindells,¹ A. T. Hindmarch,¹ A. J. Gallant,² and D. Atkinson^{1, *}

¹⁾*Department of Physics, Durham University, Durham DH1 3LE, United Kingdom*

²⁾*Department of Engineering, Durham University, Durham DH1 3LE, United Kingdom*

(Dated: 6 January 2020)

Spin current pumping from a ferromagnet through an insulating layer into a heavy metal was studied in a CoFeB/SiO₂/Pt system in relation to the thickness and interfacial structure of the insulating layer. The propagation of spin current from the ferromagnet into the heavy metal falls rapidly with sub-nanometre thicknesses of SiO₂ and is suppressed beyond a nominal thickness of 2 nm. Structural analysis shows that the SiO₂ only forms a complete barrier layer beyond around 2 nm, indicating that the presence of a discontinuous insulating barrier, and not tunneling or diffusion, explains the main observations of spin-pumping with thin insulating layers.

^{*}Electronic mail: del.atkinson@durham.ac.uk

The manipulation of spin currents across ferromagnetic (FM) and non-magnetic (NM) interfaces is key to spintronic applications and remains an active area of research^{1–3}. Precessing magnetization in a ferromagnetic layer can transfer spin angular momentum, in the form of a spin current, into an adjacent NM layer⁴, a process referred to as spin pumping. One of the main manifestations of this spin pumping mechanism is an increase in the precessional damping of a system^{5–7} and, whilst details remain to be understood, the basis of this process is well described for ferromagnetic/metallic systems^{5,8}. However, the propagation of spin current through an insulating barrier has led to conflicting results in the literature. Initial theoretical predictions of spin pumping required a transparent interface between the FM and NM layers for a large increase in damping⁹, however, early experimental results by Moriyama *et al.*¹⁰ suggested an enhancement in the damping with an insulating barrier present. This contrasts with later works by Kim *et al.*¹¹ and Mosendz *et al.*¹², who observed the suppression of spin pumping with the insertion of nano-oxide and MgO layers respectively. Studies of both Si and oxide semiconductors¹³, have also shown some suppression of spin pumping and suggest that the carriers may continue to allow spin diffusion through the barrier. Baker *et al.*¹⁴ also observed suppression of spin pumping but with dynamic exchange between two FM layers across the insulating barrier, in CoFe/MgO/Ni trilayers. Most recently, Mihalceanu *et al.*¹⁵ reported a rapid decrease in the damping due to reduced spin pumping with the addition of an ultra-thin MgO barrier layer between Fe and Pt, from which it was concluded that spin current can tunnel through a few monolayers of an insulating oxide barrier. The work was supported by transmission electron microscopy (TEM) imaging, which is limited to sampling very small areas and provides a projection of a thin 3D sample volume that may not show pinhole defects, and any defects present may be difficult to directly image¹⁶.

The discrepancies between the previous studies may be associated with the details of the multilayered structure. In particular, the nature of the interface structure in such systems is known to be important for spin-pumping^{17,18} and in the ultra-thin film regime the presence of a continuous intermediate layer needs to be established when studying such interlayer effects¹⁹. Spin pumping and $d-d$ hybridization across a FM/NM interface both lead to additional magnetic energy loss and increased precessional damping. An increase in damping linked to spin pumping across a continuous insulating layer implies some form of spin current tunneling, however, even small discontinuities, such as pinholes, within the insulating layer can allow for $d-d$ hybridization between the ferromagnetic and heavy metal layers, leading to an increase in the damping^{20,21}, and limited channels for spin current propagation. A detailed understanding of the role of structure at the

interface is therefore needed to fully characterize dynamic magnetic behavior with an insulating barrier.

This study investigates the evolution of spin-pumping from a thin-film ferromagnet into a heavy metal layer as a function of the thickness of an oxide spacer layer. The spin transport was determined by broadband FMR and the sample structure was analysed using x-ray reflectivity (XRR) in order to understand the extent of the interfacial regions between the oxide and the FM and NM layers. The study shows here that spin pumping can be fully suppressed when a complete layer of the insulating material is formed.

Enhancement of damping by spin pumping depends upon the interface and the NM material. Spin pumping leads to spin accumulation within the NM layer that decays over a characteristic length-scale, the spin diffusion length. The transparency of the interface, which governs the efficiency of spin pumping, is characterized by the effective spin-mixing conductance^{22–24}. The enhancement in damping also depends upon the thickness of both the FM and NM layers. The FM thickness dependence of the damping, α_{tot} , is commonly given by,

$$\alpha_{\text{tot}} = \alpha_0 + \frac{\gamma\hbar}{4\pi M_s t_{\text{FM}}} g_{\text{eff}}^{\uparrow\downarrow} \quad (1)$$

with α_0 the bulk intrinsic Gilbert damping parameter, $g_{\text{eff}}^{\uparrow\downarrow}$ the effective spin-mixing conductance, which is valid for a given NM thickness and other parameters. γ is the gyromagnetic ratio that can be expressed in terms of the spectroscopic g -factor using $\gamma = g\mu_B/\hbar$. The largest enhancement in the damping is obtained with a combination of a small FM thickness and a large NM thickness, i.e. above the spin diffusion length. However for in multilayered systems it may be beneficial to control the damping of the FM layers by manipulating the flow of spin current across interfaces. One method to achieve this may be to use insulating barriers, however this requires the nature of spin transport associated with an insulating barrier to be understood

Magnetron sputtering was used to grow a series of samples varying the SiO_2 thickness in a $\text{CoFeB}(10\text{ nm})/\text{SiO}_2(0 - 5\text{ nm})/\text{Pt}(10\text{ nm})$ structure, along with a reference samples with no Pt. Dynamic and direct structural measurements on the reference samples can be found in supplemental material.

XRR was used to extract interfacial structure information. This method measures over a large area, of the order of square centimeters, unlike transmission electron microscopy, providing an averaged view of both the layers and interfaces within a sample. Figure 1 shows examples of both

the measured reflectivity data and the best-fitting simulations obtained using the GenX code²⁵. The scattering length density profiles were extracted from the best-fitting model for a sample of CoFeB(10 nm)/SiO₂(2 nm)/Pt(10 nm) and CoFeB(10 nm)/SiO₂(5 nm)/Pt(10 nm). The interfaces width in such multilayered structures results from a combination of topographical roughness of interface between the layers and some chemical intermixing between these different layers, here the interface width between the insulating and FM layers largely reflects chemical intermixing across the interface. A value of the interface width can be estimated from the slope of the scattering length density (SLD) where it changes from 90% to 10% of its value from one layer to the next. For the CoFeB and SiO₂ interface, this analysis gives an interface width of 2.4 nm, below this thickness the SiO₂ layer is discontinuous.

The damping was obtained from measurements of magnetic field-swept FMR as a function of SiO₂ thickness. In this setup, the sample was placed face down onto an impedance-matched microstripline, driven at fixed excitation frequency, f , by an RF signal generator, with an external biasing magnetic field applied parallel to the transmission line and hence orthogonal to the RF excitation field. Helmholtz coils were used to modulate the bias field and the time-varying output voltage of a diode power detector across the line, proportional to the field derivative of the transmitted RF power, and hence microwave absorption, χ'' , by the sample, was measured using a lock-in amplifier. The inset in figure 2 (a) shows typical spectra around resonance as a function of magnetic field for various excitation frequencies, f .

The relationship between the field swept line width, ΔH , and resonant frequency allows for the separation of intrinsic and extrinsic contributions to the damping using,

$$\Delta H = \Delta H_0 + \frac{4\pi\alpha}{\gamma} f, \quad (2)$$

where $4\pi\alpha/\gamma$ is the intrinsic line width and ΔH_0 is the extrinsic line width, which is related to defects and leads to two-magnon scattering. An example fit to the line width data used to separate these contributions to the damping is shown in figure 2 (a).

The effect of increasing the thickness of a SiO₂ spacer layer on both the intrinsic and extrinsic contributions to the precessional damping in CoFeB(10 nm)/SiO₂(x nm)/Pt(10 nm) multilayers is shown in figure 2(b) and (c). As the nominal thickness of the oxide layer between the ferromagnet and the heavy metal spin-sink increases, the intrinsic line width decreases. This decrease is at a similar rate to that observed for an MgO spacer layer¹⁵. The intrinsic damping decreases towards the value in the case where no spin-sink is present, as indicated on the figure by the orange square

data point. No change in intrinsic damping is observed with varying the SiO_2 thickness without a Pt layer. The continued enhancement of damping with thin insulating barrier thicknesses was previously attributed to tunneling of spin current through the insulating spacer layer.

However, an understanding of the interfacial structure is important. As shown in figure 3, by superimposing the normalised structural SLD profile of the $\text{CoFeB}/\text{SiO}_2$ interface on the same nominal SiO_2 thickness-axis as for the damping, the relationship between the structure of the insulating layer and the measured damping response can be compared. At low SiO_2 thicknesses (below 2.4 nm) the SiO_2 layer is discontinuous, enabling some localised direct contact and $d-d$ hybridization between the ferromagnet and the heavy metal (HM), where the spacer layer is incomplete, and creates direct pathways for propagation of spin current from the ferromagnet into the spin-sink. These two mechanisms enhance the damping above that of the pure ferromagnet²⁰, but decrease rapidly as the area of HM in direct contact with the FM is reduced. However, when the insulating spacer layer continuously covers the ferromagnet, above 2.4 nm, there is no measured enhancement of the intrinsic damping from the heavy metal layer.

The effects of the discontinuous interface is also observed in the SiO_2 thickness dependence of the extrinsic contribution to the damping, see figure 3(b). An increase in the extrinsic contribution to the line width indicates an increase in defects that mediate two-magnon scattering processes. As a function of SiO_2 thickness the extrinsic contribution increases in a single large step with the thinnest oxide layer and then decreases as the thickness increases further, this decrease is comparable with the form of the scattering length density. The extrinsic contribution provides evidence further supporting the interpretation of the nominal thickness dependence as a consequence of the presence of a discontinuous insulating layer, as it has been previously shown that discontinuous coverage of a ferromagnet with a heavy metal layer leads to enhanced extrinsic damping²¹. An slight enhancement in extrinsic damping was also found without a Pt layer, which may be attributed to partial oxidation of the FM surface due to a discontinuous interface. The common dependence of intrinsic and extrinsic damping upon the discontinuous SiO_2 is further evidenced by the linear correlation between the extrinsic and intrinsic contributions for samples lacking a full surface coverage of the SiO_2 layer (i.e. below 2.4nm), as shown in figure 3(c). Here, as discussed, regions with a low surface coverage allow for a large increase in both the extrinsic and intrinsic contributions, which are both suppressed with the same functional form as the layer becomes complete. Direct surface measurements are unable to distinguish between defects such as pinholes which would lead to this effect and topographical roughness, due to the lack of element specificity.

In conclusion, the link between the structure of the interface and the spin transport with a SiO_2 spacer layer was examined. It was found that spin-pumping was observed for nominal SiO_2 thicknesses up to around 2 nm, but this correlates with the length-scale corresponding to the interface width of the barrier, such that, structurally the insulating layer was discontinuous when spin-pumping was observed and no enhancement of the damping was measured when the SiO_2 layer was complete (>2.4 nm). Thus, the experimentally observed spin-pumping signals with ultra thin insulators are due to the discontinuous insulating layer rather than requiring models involving tunneling of pure spin-current. The incomplete SiO_2 layer also leads to enhanced extrinsic damping resulting from direct coupling between the FM and HM layers when the insulating layer is discontinuous. It is also shown that when the SiO_2 layer is continuous it represents a significant barrier to spin transport, which allows for the suppression of spin current in multilayered structures.

SUPPLEMENTARY MATERIAL

See supplementary material for dynamic and direct structural measurements on the $\text{CoFeB}/\text{SiO}_2$ bilayers.

ACKNOWLEDGEMENTS

Funding is acknowledged from EPSRC for the studentship for CR Swindells 1771248, Ref. EP/P510476/1. Data presented within this article can be found at <https://doi:10.15128/r2cf95jb46b>

REFERENCES

- ¹I. Zutic, J. Fabian, and S. D. Sarma, Rev. Mod. Phys. **76**, 323 (2007).
- ²A. Hoffmann, IEEE Trans. Magn. **49**, 5172 (2013).
- ³S. Azzawi, A. T. Hindmarch, and D. Atkinson, J. Phys. D. Appl. Phys. **50**, 473001 (2017).
- ⁴Z. Q. Qiu, A. Tan, L. R. Shelford, P. S. Keatley, P. Shafer, J. Li, E. Arenholz, J. X. Deng, C. Hwang, G. van der Laan, and R. J. Hicken, Phys. Rev. Lett. **117**, 076602 (2016).
- ⁵Y. Tserkovnyak, A. Brataas, and G. E. Bauer, Phys. Rev. B **66**, 224403 (2002).
- ⁶J. C. Rojas-Sánchez, N. Reyren, P. Laczkowski, W. Savero, J. P. Attané, C. Deranlot, M. Jamet, J. M. George, L. Vila, and H. Jaffrès, Phys. Rev. Lett. **112**, 106602 (2014).

- ⁷M. Caminale, A. Ghosh, S. Auffret, U. Ebels, K. Ollefs, F. Wilhelm, A. Rogalev, and W. E. Bailey, *Phys. Rev. B* **94**, 014414 (2016).
- ⁸C. Swindells, A. T. Hindmarch, A. J. Gallant, and D. Atkinson, *Phys. Rev. B* **99**, 064406 (2019).
- ⁹A. Brataas, Y. Tserkovnyak, G. E. W. Bauer, and B. I. Halperin, *Phys. Rev. B* **66**, 060404 (2002).
- ¹⁰T. Moriyama, R. Cao, X. Fan, G. Xuan, B. K. Nikolić, Y. Tserkovnyak, J. Kolodzey, and J. Q. Xiao, *Phys. Rev. Lett.* **100**, 067602 (2008).
- ¹¹D. H. Kim, H. H. Kim, and C. Y. You, *Appl. Phys. Lett.* **99**, 072502 (2011).
- ¹²O. Mosendz, J. E. Pearson, F. Y. Fradin, S. D. Bader, and A. Hoffmann, *Appl. Phys. Lett.* **96**, 022502 (2010).
- ¹³C. H. Du, H. L. Wang, Y. Pu, T. L. Meyer, P. M. Woodward, F. Y. Yang, and P. C. Hammel, *Phys. Rev. Lett.* **111**, 247202 (2013).
- ¹⁴A. A. Baker, A. I. Figueroa, D. Pingstone, V. K. Lazarov, G. Van Der Laan, and T. Hesjedal, *Sci. Rep.* **6**, 35582 (2016).
- ¹⁵L. Mihalceanu, S. Keller, J. Greser, D. Karfaridis, K. Simeonidis, G. Vourlias, T. Kehagias, A. Conca, B. Hillebrands, and E. T. Papaioannou, *Appl. Phys. Lett.* **110**, 252406 (2017).
- ¹⁶A. Thomas, V. Drewello, M. Schäfers, A. Weddemann, G. Reiss, G. Eilers, M. Münzenberg, K. Thiel, and M. Seibt, *Appl. Phys. Lett.* **93**, 152508 (2008).
- ¹⁷M. Tokaç, S. A. Bunyayev, G. N. Kakazei, D. S. Schmool, D. Atkinson, and A. T. Hindmarch, *Phys. Rev. Lett.* **115**, 056601 (2015).
- ¹⁸A. Ganguly, S. Azzawi, S. Saha, J. A. King, R. M. Rowan-Robinson, A. T. Hindmarch, J. Sinha, D. Atkinson, and A. Barman, *Sci. Rep.* **5**, 17596 (2015).
- ¹⁹R. M. Rowan-Robinson, A. A. Stashkevich, Y. Roussigné, M. Belmeguenai, S. M. Chérif, A. Thiaville, T. P. Hase, A. T. Hindmarch, and D. Atkinson, *Sci. Rep.* **7**, 16835 (2017).
- ²⁰E. Barati, M. Cinal, D. M. Edwards, and A. Umerski, *Phys. Rev. B - Condens. Matter Mater. Phys.* **90**, 014420 (2014).
- ²¹S. Azzawi, A. Ganguly, M. Tokaç, R. M. Rowan-Robinson, J. Sinha, A. T. Hindmarch, A. Barman, and D. Atkinson, *Phys. Rev. B* **93**, 054402 (2016).
- ²²W. Zhang, W. Han, X. Jiang, S. H. Yang, and S. S. Parkin, *Nat. Phys.* **11**, 496 (2015).
- ²³O. R. Sulymenko, O. V. Prokopenko, V. S. Tiberkevich, A. N. Slavin, B. A. Ivanov, and R. S. Khymyn, *Phys. Rev. Appl.* **8**, 064007 (2017).
- ²⁴M. Weiler, M. Althammer, M. Schreier, J. Lotze, M. Pernpeintner, S. Meyer, H. Huebl, R. Gross, A. Kamra, J. Xiao, Y. T. Chen, H. Jiao, G. E. Bauer, and S. T. Goennenwein, *Phys. Rev. Lett.*

111, 176601 (2013).

²⁵M. Björck and G. Andersson, J. Appl. Crystallogr. **40**, 1174 (2007).

FIGURES

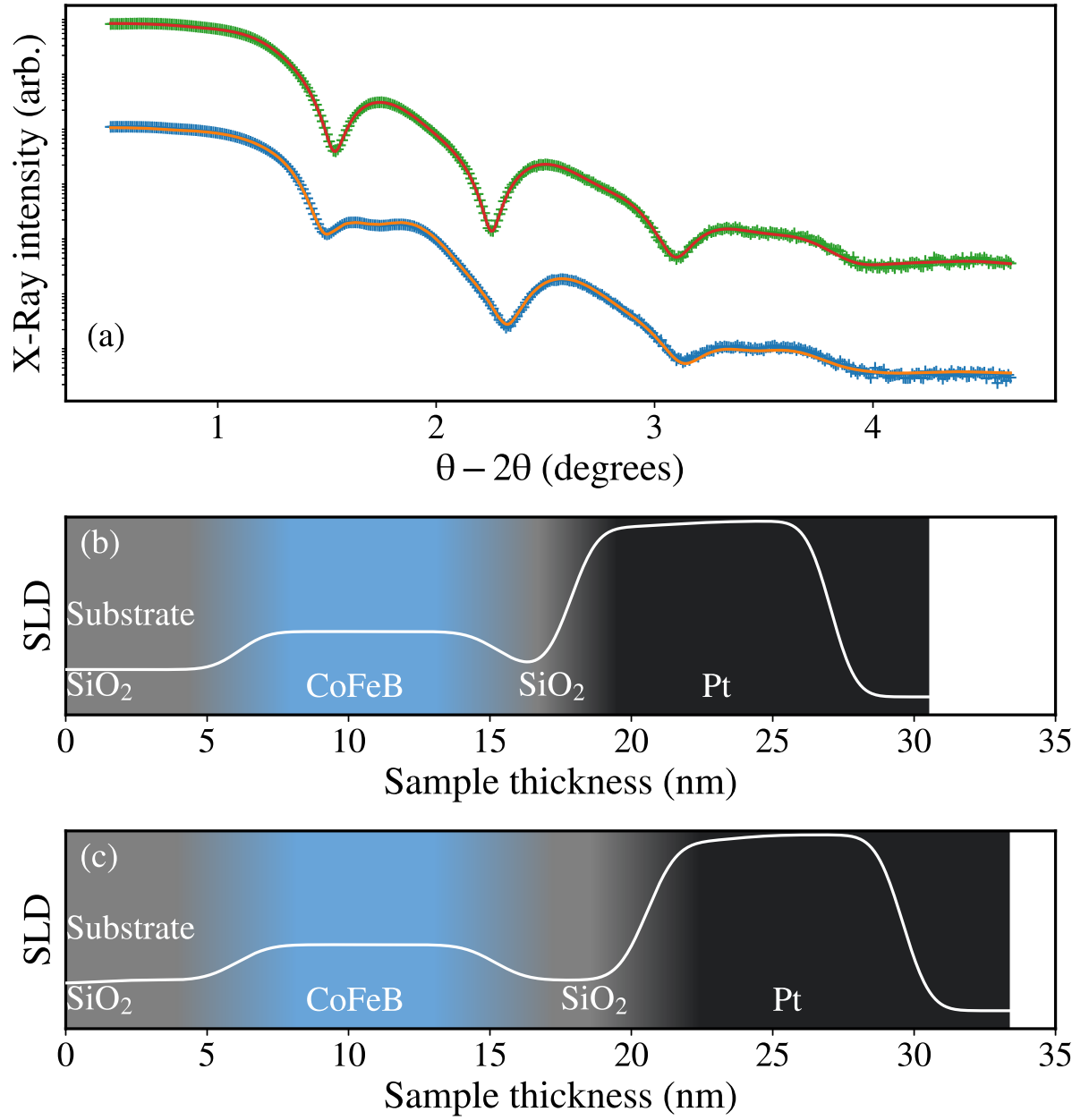
FIG. 1. (a) XRR Data and best fit for CoFeB(10 nm)/SiO₂(2 nm)/Pt(10 nm) (top) and CoFeB(10 nm)/SiO₂(5 nm)/Pt(10 nm) (bottom). (b) Real part of the scattering length density (SLD) profile from the best fit to the data for the 2 nm oxide barrier. (c) Same as (b) for the 5 nm barrier.

FIG. 2. (a) Inset shows absorption derivative profiles at four frequencies with fits, obtained from lock-in amplifier field-swept FMR, for CoFeB(24 nm)/Pt(10 nm)/SiO₂(5 nm). Rest of (a) shows measured line width from field-swept FMR, fitted to eq. 2 to extract both intrinsic and extrinsic damping contributions. (b) Decrease in intrinsic contributions to FMR line width as a function of SiO₂ thickness for CoFeB(10 nm)/SiO₂(*x* nm)/Pt(10 nm) (blue circles) with reference sample without platinum (orange square). (c) Decrease in extrinsic contributions as a function of SiO₂ thickness, where the orange square at 0 nm denotes a reference sample with no SiO₂, and at 5 nm denotes reference sample without Pt

FIG. 3. (a) As figure 2 (b) , but with extracted SLD for the 5 nm SiO₂ barrier from fig 1(c) superimposed shown in red dashed lines. The horizontal grey bar indicates the damping equivalent to that of the ferromagnetic layer only. (b) As figure 2 (c) with SLD for a 5 nm SiO₂ barrier superimposed on top given by the red dashed line. (c) Correlation between the intrinsic and extrinsic contributions for samples without a full surface coverage of the insulating layer.

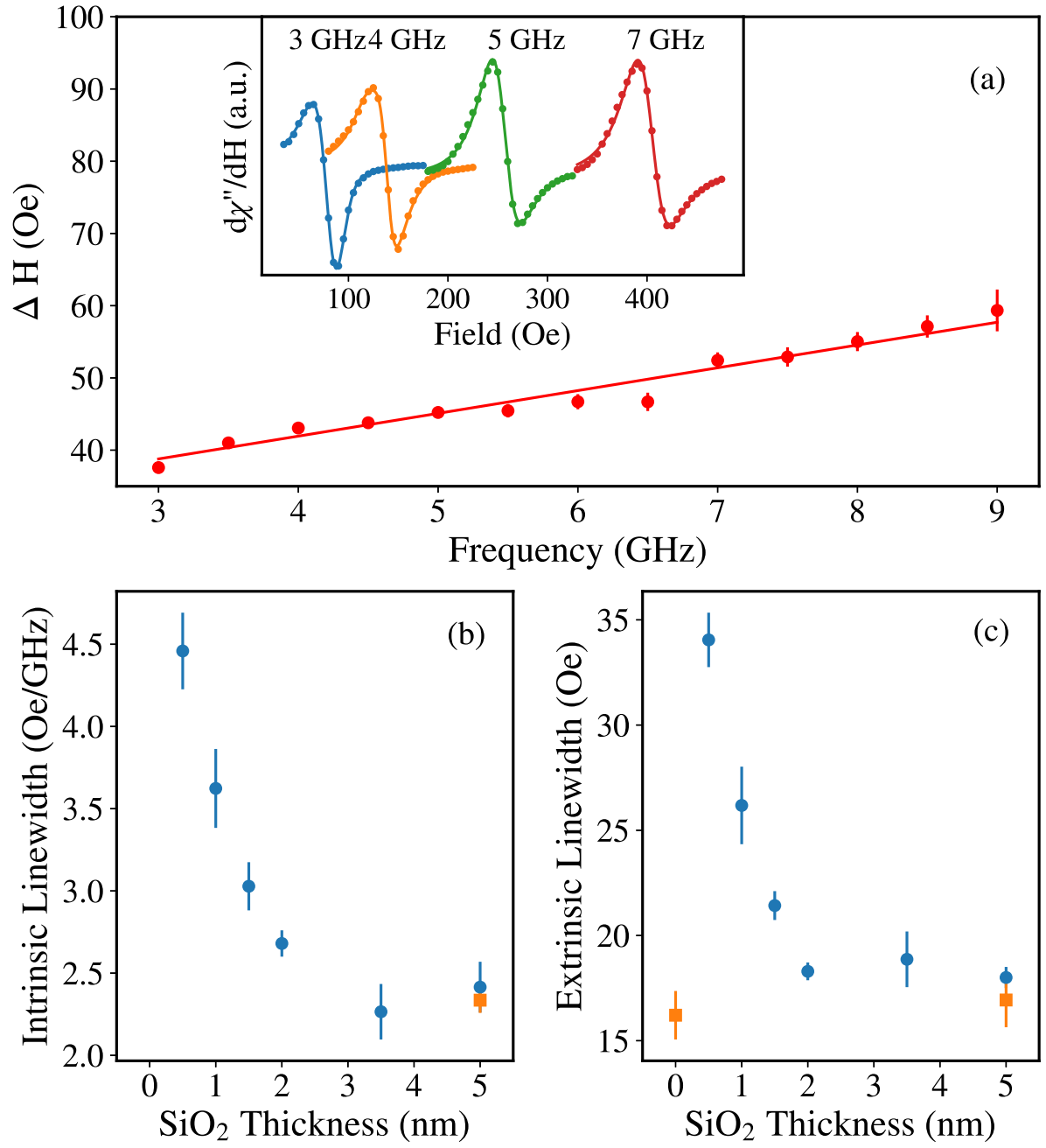
This is the author's peer reviewed, accepted manuscript. However, the online version of record will be different from this version once it has been copyedited and typeset.

PLEASE CITE THIS ARTICLE AS DOI: 10.1063/1.5119787



This is the author's peer reviewed, accepted manuscript. However, the online version of record will be different from this version once it has been copyedited and typeset.

PLEASE CITE THIS ARTICLE AS DOI: 10.1063/1.5119787



This is the author's peer reviewed, accepted manuscript. However, the online version of record will be different from this version once it has been copyedited and typeset.

PLEASE CITE THIS ARTICLE AS DOI: 10.1063/1.5119787

